HAL open science

Elaboration of multimodal ligands based on BOX units: Toward full zinc release in Zn(II) complexes by external stimulation

Youssef Aidibi, Magali Allain, Abdelkrim El-Ghayoury, Philippe Leriche, Lionel Sanguinet

▶ **To cite this version:**

Youssef Aidibi, Magali Allain, Abdelkrim El-Ghayoury, Philippe Leriche, Lionel Sanguinet. Elaboration of multimodal ligands based on BOX units: Toward full zinc release in Zn(II) complexes by external stimulation. Dyes and Pigments, 2021, 193, pp.109476. 10.1016/j.dyepig.2021.109476 . hal-03766482

HAL Id: hal-03766482

https://hal.science/hal-03766482v1

Submitted on 13 Jun 2023

HAL is a multi-disciplinary open access archive for the deposit and dissemination of scientific research documents, whether they are published or not. The documents may come from teaching and research institutions in France or abroad, or from public or private research centers.

L'archive ouverte pluridisciplinaire **HAL**, est destinée au dépôt et à la diffusion de documents scientifiques de niveau recherche, publiés ou non, émanant des établissements d'enseignement et de recherche français ou étrangers, des laboratoires publics ou privés.

Distributed under a Creative Commons Attribution - NonCommercial 4.0 International License

Version of Record: https://www.sciencedirect.com/science/article/pii/S0143720821003429
Manuscript_9e72d1d3790465eb64b0cac55bdacad5

Elaboration of multimodal ligands based on BOX units: toward full zinc release in Zn(II) complexes by external stimulation

Youssef Aidibi, Magali Allain, Abdelkrim El-Ghayoury, Philippe Leriche and Lionel Sanguinet*
Univ Angers, CNRS, MOLTECH – Anjou, SFR matrix, F-49000 Angers, France
lionel.sanguinet@univ-angers.fr; +33241735374

Abstract

The development of molecular switches such as photochromic and electrochromic systems still represents a major concern in numerous application fields. If numerous pure organic switch families have been explored so far, concerning the coordination compounds, the choice seems more limited. In this context, we are exploring the possibility to elaborate a new addressable ligand family based on benzazolo-oxazolidine (BOX) moiety, a poorly investigated switch family, known for its acido-, electro- and photochromism properties. As proof of concept, two ligands bearing a BOX moiety were prepared using a pyridine as metal binding site after what corresponding Zn(II) complexes were synthesized and characterized. The acido-, electro- and photochemical behaviors of the free ligand as well as complexes were studied. This study reveals a subtle and interesting tautomeric equilibrium between oxazolidine ring opening and pyridine protonation whatever the nature of the stimulation. More interestingly, it conducts to observe the possibility to catch and release zinc ion on demand by using two external and orthogonal stimulations.

Keywords

Photoresponsiveness ; electrochomism ; halochromism ; zinc complex

1. Introduction

The elaboration of molecular systems allowing a modulation of their molecular properties as response to an external stimulation continues to rise a growing attention from a large scientific community. Depending of *(i)* the nature of the modulated molecular properties and (*ii*) the kind of stimulus, such systems can find applications in numerous fields such as optical data storage and molecular logic gate,[1] medical imaging,[2] magnetism,[3] and chemical sensors to name a few. Among these last, the elaboration of photochromic systems, able to undergo a reversible transformation under light irradiation has attracted much attention. Thus, amongst the numberless pure organic photochromic materials elaborated and studied,[4] the diarylethene (DAE),[5, 6]

© 2021 published by Elsevier. This manuscript is made available under the CC BY NC user license
https://creativecommons.org/licenses/by-nc/4.0/

azobenzene[7] and spiropyrans[8, 9] based systems represent certainly the most three widespread photochromic families. Allowing the modulation between only two discrete levels of properties (referenced generally as On and Off states), several of these motifs may be associated in order to elaborate molecular systems exhibiting a higher degree of complexity.[10] However, as the multistep synthesis of organic compounds associating n switchable units appeared often tricky and hazardous, the resulting structures did not necessary allow the awaited expansion of the number of metastable states (theoretically up to 2^n). In fact, several reviews were dedicated to multi-chromophoric molecular systems especially based on DAE unit.[6, 10, 11] In these multi-photochromic systems, different behaviors can be observed ranging from the perfect selectivity of the switch addressability to the complete inhibition of the photochromic properties of the DAE as function of the status of the other commutable unit (generally referenced as gated photochromism). [11, 12]

In this context, the coordination chemistry offers an interesting approach to circumvent some of these issues. First, it provides an efficient and convenient way to elaborate multi-chromophoric systems as exemplified by the large variety of DAE multimers using a metallic center as connector.[10] Second, the resulting complexes could lead to the combination of several functionalities by gathering, for example, an electroactive organometallic moiety and a photoresponsive ligand,[13, 14] or, as more recently shown by Crassous and Rigaut teams, by connecting two ligands with complementary properties merging photochromic and chiroptical properties.[15] To obtain such systems, the classical approach consists in functionalizing a classical nitrogen-based binding unit (pyridine, bi-pyridine, ter-pyridine or phenanthroline), in most cases, by a DAE as photochromic unit or, more rarely, by spiropyran and spiroxazine moieties.[16, 17] Photo-responsive metal complexes featuring an azo-aryl function were also reported. In these cases, the photochromic and electrochemical properties were strongly affected by the strength of interactions between azo and metal units and, then, the obtainment of the multi-functional system was not assured.[17-21] From these observation, it may be concluded that the elaboration of photo-addressable metal complexes may lay on a limited choice of structures. In addition, a similar situation is also observed from systems incorporating electro-active ligands. Despite systems including "non-innocent ligand"[22] for which the electrostimulation conducts to redox state change of the metal center, most of the electro-responsive complexes are elaborated from ligands incorporating a tetrathiafulvalene (TTF) as redox active unit.[23, 24]

In this context, we report here on our efforts to develop a new family of ligands based on indolino-oxazoline derivatives (referenced later as BOX), a poorly investigated family of multi-modal addressable units, on their coordination behavior as well as on properties of corresponding

complex. Indeed, the opening and closure of the oxazolidine ring can be induced using indifferently three different kinds of stimulation and results to nice photo-, electro- and acido-chromic performances.[25] Up to now, restricted to the elaboration of pure organic molecular systems mainly dedicated to the development of nonlinear optical (NLO) switches, this promising unit was, to the best of our knowledge, never involved in supramolecular assembly neither in metallic complexes. To fulfill this gap, we have successfully prepared two dyads incorporating a BOX unit associated to a pyridine moiety as the simplest nitrogen-based binding unit and studied their coordination behavior toward Zinc(II) as well as the switching properties of the resulting system.

2. Experimental

2.1. General

Flash chromatography was performed with analytical grade solvents using Aldrich silica gel (technical grade, pore size 60 Å, 230-400 mesh particle size). Flexible plates ALUGRAM® Xtra SIL G UV254 from MACHEREY-NAGEL were used for TLC. All chemical reagents were used as received form commercial suppliers (Sigma-Aldrich or Acros).

The NMR spectra were recorded with a Bruker AVANCE III 300 (^{1}H, 300 MHz and ^{13}C, 75 MHz) using $CDCl_3$ as solvent. Chemical shifts are reported in ppm relative to the solvent residual value: $\delta = 7.26$ for ^{1}H NMR and $\delta = 77.16$ for ^{13}C NMR. Coupling constants are reported in Hz and rounded to the nearest 0.1 Hz.

Infrared spectra were recorded on a Bruker Vertex 70 spectrometer. UV-Vis spectra were performed with a Perkin Elmer 950 spectrometer from solutions in ACN (HPLC grade from VWR chemicals) in presence of Chlorobenzene (99+% form ACROS). In agreement with our previous studies, titrations were performed using either daily fresh prepared $NOSbF_6$ (Sigma-Aldrich) solution in ACN or a HCl solution in ACN prepared by successive dilution from brand new aqueous solution of HCl (37% from VWR chemicals). UV Irradiation were performed directly in spectroscopy cells by using 254 nm lamp (6W) suitable for thin layer chromatography. The Mass spectra were recorded using BIFLEX III Bruker Daltonics spectrometer (MALDI-TOF, dithranol matrix) and Elemental analysis (EA) was performed on a Thermo Scientific flash 2000 elemental analyzer.

The electrochemistry studies were performed on dichloromethane solutions (HPLC grade) with tetra-n-butylammonium hexafluorophosphate (TBAP, electrochemical grade from Fluka) as the support electrolyte (0.1M) under a dry and oxygen-free atmosphere (H_2O < 1 ppm, O_2 < 1 ppm). Cyclic voltammetry (CV) was performed in a three-electrode cell equipped with a platinum

millielectrode as working electrode, a platinum wire counter-electrode and a silver wire used as a quasi-reference electrode. The voltammograms were recorded on a potentiostat/galvanostat (BioLogic – SP150) driven by the EC-Lab software with positive feedback compensation. All of them were calibrated *versus* Ferrocene/Ferrocenium oxidation potential (+0.405V vs SCE or +0.425V vs Ag/AgCl).[26]

2.2. Synthesis

As previously reported,[27] both trimethyl indolino[2,1,b]oxazolidine derivatives were prepared according to the following procedure:

General procedure: A mixture of indolenine derivative (86.9 mmol) and 2-iodoethanol (130.4 mmol, 1.5 eq.) in toluene (135 mL) was refluxed overnight. After cooling to room temperature, the precipitate was filtered off, washed with cold Et_2O (3x30ml) and acetone (3x30ml) and dried to afford corresponding indoleninium iodide salt which was used in the next step without further purification.

To a suspension of indoleninium iodide salt (70.5 mmol) in water (500 mL), 250 mL of aqueous NaOH solution (2M) were added under vigorous agitation at room temperature. After 30 min, the crude material was extracted with Et_2O (3x1000 mL). The organic phases were combined, washed with water (2 times), brine (1 time) and dried over $MgSO_4$. The solvent was removed under reduced pressure to afford the corresponding trimethyl indolino[2,1-b]oxazolidine derivative as a brown oil which was used without further purification.

2,3,3-trimethylindolino[2,1-b]oxazoline (3a) : Product was isolated as a brown oil (93%). ^{1}H NMR (300 MHz, $CDCl_3$) δ (ppm) 7.14 (td, J = 7.7, 1.2 Hz, 1H), 7.08 (d, J = 7.4 Hz, 1H), 6.93 (td, J = 7.4, 0.8 Hz, 1H), 6.77 (d, J = 7.8 Hz, 1H), 3.90 – 3.43 (m, 4H), 1.43 (s,3H), 1.39 (s, 3H), 1.18 (s, 3H).

2,3,3,5-tetramethylindolino[2,1-b]oxazoline (3b) : Product was isolated as a brown oil (91%). ^{1}H NMR (300 MHz, $CDCl_3$) δ (ppm) 6.93 (d, J = 7.9 Hz, 1H), 6.89 (s, 1H), 6.66 (d, J =7.9 Hz, 1H), 3.91-3.42 (m, 4H), 2.30 (s, 3H), 1.41 (s, 3H), 1.38 (s, 3H), 1.17 (s,3H).

General procedure for the elaboration of the ligands: A mixture of 4-pyridinecarboxaldehyde (2.3 mmol) and corresponding indolino-oxazolidine (2.8mmol) were dissolved in a little amount of DCM. 1g of technical grade silica was suspended and the solvent was removed under reduced pressure. The resulting reaction mixture was heated under stirring at 100°C during 10 min. After cooling down to room temperature, the crude material was directly purified by flash chromatography (PE/ EtOAc, 3/7).

(E)-9,9-dimethyl-9a-(2-(pyridin-4-yl)vinyl)-2,3,9,9a-tetrahydrooxazolo[3,2-a]indole; 4a: Product was isolated as a yellow solid (496 mg, 73%). m.p.: 115°C

^{1}H NMR (300 MHz, $CDCl_3$) δ (ppm): 8.58 (dd, *J* = 4.5, 1.6 Hz, 2H), 7.31 (dd, *J* = 4.6, 1.5 Hz, 2H), 7.22 – 7.15 (m, 1H), 7.09 (dd, *J* = 7.4, 0.9 Hz, 1H), 6.96 (td, *J* = 7.4, 1.0 Hz, 1H), 6.83 (dd, *J* = 11.9, 6.6 Hz, 2H), 6.53 (d, *J* = 15.9 Hz, 1H), 3.85 – 3.37 (m, 5H), 1.46 (s, 3H), 1.17 (s, 3H).. ^{13}C NMR (75 MHz, $CDCl_3$) δ (ppm): 150.3, 150.2, 143.8, 139.5, 131.5, 130.1, 127.8, 122.4, 122.0, 121.3, 112.1, 109.5, 63.8, 50.2, 48.2, 28.4, 20.5. IR $\bar{\upsilon}$ = 2962, 2889, 1595, 1476, 1454, 1292, 1149, 975, 750 cm^{-1} Anal. calcd for $C_{19}H_{20}N_2O$: C, 78.05; H, 6.89; N, 9.58, found: C, 77.80; H, 6.75; N, 9.45. cm^{-1} . MS (MALDI-TOF): *m/z* calcd. For $C_{19}H_{20}N_2O$: 292.1576 [M+H] ; found: 292.1574. Anal. calcd for $C_{19}H_{22}N_2O$: C, 78.05; H, 6.89; N, 9.58, found: C, 77.80; H, 6.75 N, 9.45.

(E)-7,9,9-trimethyl-9a-(2-(pyridin-4-yl)vinyl)-2,3,9,9a-tetrahydrooxazolo[3,2-a]indole; 4b*:* Product was isolated as a yellow solid (627 mg, 88%). m.p.: 114-115°C. ^{1}H NMR (300 MHz, $CDCl_3$) δ (ppm) 8.57 (d, *J* = 6.0 Hz, 2H), 7.30 (d, *J* = 6.1 Hz, 2H), 6.99 (d, *J* = 7.9 Hz, 1H), 6.90 (s, 1H), 6.83 (d, *J* = 15.9 Hz, 1H), 6.71 (d, *J* = 7.9 Hz, 1H), 6.53 (d, *J* = 15.9 Hz, 1H), 3.83 – 3.34 (m, 4H), 2.32 (s, 3H), 1.45 (s, 3H), 1.16 (s, 3H). ^{13}C NMR (75 MHz, $CDCl_3$) δ (ppm) 150.3, 148.0, 143.8, 139.6, 131.6, 131.4, 130.0, 128.3, 123.16, 121.3, 111.9, 109.8, 63.8, 50.4, 48.2, 28.4, 21.1, 20.4. IR $\bar{\upsilon}$ = 2967, 2882, 1737, 1413 cm^{-1}. MS (MALDI-TOF): *m/z* calcd. For $C_{20}H_{22}N_2O$: 306.1732 [M+H] ; found: 306.1728. Anal. calcd for $C_{20}H_{22}N_2O$: C, 78.40; H, 7.24; N, 9.14, found: C, 78.13; H, 7.04; N, 9.3.

General procedure for the elaboration of Zinc complexes: In a test tube, a solution of desired ligand (0.147 mmol) in CH_2Cl_2 (5 mL) was mixed with a solution of $ZnCl_2$ (0.073 mmol) in CH_3CN (5 mL) and ultra-sonicated for 2 min. On top of the resulting solution a layer of diethyl ether was added, which led to a precipitate after one week. The desired compound was filtered off, washed with diethyl ether and dried under vacuum.

Dichlorobis-[9,9-dimethyl-9a-(2-(pyridin-4-yl)vinyl)-2,3,9,9a-tetrahydrooxazolo[3,2-a]indole]zinc(II), 5a*:* Product was isolated as yellow solid (69%).

^{1}H NMR (300 MHz, CD_3CN) δ (ppm): 8.66 (dd, *J* = 5.0, 1.5 Hz, 2H), 7.74 (dd, *J* = 5.0, 1.6 Hz, 2H), 7.24 – 7.17 (m, 1H), 7.15 (dd, *J* = 7.4, 0.8 Hz, 1H), 6.96 (ddd, *J* = 10.6, 3.5, 2.1 Hz, 2H), 6.89 (d, *J* = 7.8 Hz, 1H), 6.78 (d, *J* = 15.9 Hz, 1H), 3.82 – 3.36 (m, 4H), 1.44 (s, 3H), 1.15 (s, 3H). IR $\bar{\upsilon}$ = 2960, 1612, 1477, 1275, 749 cm^{-1}. Anal. calcd for $C_{40}H_{44}N_4O_2Cl_2Zn$: C, 63.30; H, 5.59; N, 7.77, found: C, 62.92; H, 5.44; N, 7.35.

Dichlorobis-[7,9,9-trimethyl-9a-(2-(pyridin-4-yl)vinyl)-2,3,9,9a-tetrahydrooxazolo[3,2-a]indole]zinc(II) 5b: Product was isolated as yellow single crystals (78%).

^{1}H NMR (300 MHz, CD_3CN) δ (ppm): 8.61 (d, *J* = 6.5 Hz, 2H), 7.68 (d, *J* = 6.5 Hz, 2H), 6.97 (d, *J* = 7.9 Hz, 1H), 6.94 (s, 1H), 6.90 (d, *J* = 16.1 Hz, 1H), 6.73 (dd, *J* = 11.9, 4.0 Hz, 2H), 3.77 – 3.28 (m, 6H), 2.27 (s, 3H), 1.38 (s, 3H), 1.09 (s, 3H). ^{13}C NMR (75 MHz, CD_3CN) δ (ppm):149.7, 149.3, 149.0, 140.5, 136.4, 132.0, 129.6, 129.0, 124.0, 112.8, 110.5, 64.4, 50.8, 48.8, 28.5, 20.9, 20.6. IR $\bar{\upsilon}$ = 2958, 1613, 1489, 811 cm^{-1}. Anal. calcd for $C_{40}H_{44}N_4O_2Cl_2Zn$: C, 64.13; H, 5.92; N, 7.48, found: C, 62.15; H, 5.75; N, 7.14.

2.3. Crystal data collection and processing.

X-ray single-crystal diffraction data for free ligand, **4b,** and its zinc(II) complex, **5b**, were collected on an Agilent SuperNova diffractometer equipped with Atlas CCD detector and mirror monochromated micro-focus Cu-Kα radiation (λ = 1.54184 Å). The two structures were solved by direct methods, expanded and refined on F^2 by full matrix least-squares techniques using SHELX97 programs (G.M. Sheldrick, 1998). All non-H atoms were refined anisotropically and the H atoms were included in the calculation without refinement. Multi-scan empirical absorption was corrected using the CrysAlisPro program (CrysAlisPro, Agilent Technologies, V1.171.37.35g, 2014). Crystallographic data for the structural analysis have been deposited at the Cambridge Crystallographic Data Centre, CCDC 2040158 for ligand **4b** and CCDC 2040159 for the zinc complex **5b**.

2.4. Quantum chemical calculations.

Full geometry optimizations of compound **4b** and corresponding zinc complex **5b** were performed based on density functional theory (DFT) using the classic B3LYP functional with the 6-311G(d) basis set. All optimized structures correspond to stationary points on the potential energy surfaces, as confirmed by only real vibrational frequencies. Linear optical properties were determined at the time-dependent DFT level using the B3LYP functional with the larger 6-311+G(d) basis set. Solvent (acetonitrile) effects were included in all calculations by means of the polarizable continuum model in its integral equation formalism (IEF-PCM).[28]

3. Results and discussion

3.1. Synthesis

To prepare the photo-active ligands based on BOX unit, a classical convergent synthesis strategy was envisioned. Corner stone of this strategy, the condensation reaction between a trimethylindolino[2,1-b]oxazolidine derivative and some aromatic aldehyde is well-documented and was reported for numerous aromatic hydrocarbon in various experimental conditions (protic

and aprotic solvents, acid or basic catalysis, solvent-free conditions).[25, 29, 30] Surprisingly, the association of BOX with an aromatic nitrogen heterocycle was remained unexplored up to now. Only few examples using heterocycles were reported and, to the best of our knowledge, are limited to thiophene and furan derivatives. For such reason, the condensation reaction with pyridinecarboxaldehyde was carried out using a silica-mediated procedure known to improve the reactivity of the trimethylindolino[2,1-b]oxazolidine derivative.[30] Starting from an equimolar mixture of **3a** (**3b**) and 4-pyridinecarboxaldehyde, the formation of the desired ligands **4a (4b)** was well noticed after heating during 10 min. Unfortunately, the full conversion of the aldehyde could not be reached even under prolonged heating times and its presence in the reaction mixture led to inextricable purification difficulties. By using a slight excess of BOX (1.2 equivalent) the reaction equilibrium can be displaced and the purification of target molecules was greatly facilitated allowing to obtain ligands **4a** and **4b** in excellent yields (73 and 88% respectively).

In order to prepare a first series of photo-responsive metal complexes based on BOX, our choice fell on zinc(II) as metallic ion. Indeed, this metal choice presents several advantages such as a low cost, no stereochemistry preference arising from ligand field stabilization effects, and the preparation of corresponding complex is easy and well documented especially from pyridine based ligands.[31] More important, the absence of low-energy metal-to-ligand or metal d–d electronic transitions, its lack of redox activity and finally its diamagnetic properties[32] present some important advantage for the study of the electro- and photo-induced transformations of our multi-responsive ligand especially by NMR spectroscopy.[33] Using classical experimental conditions with $ZnCl_2$,[34] the two different zinc complexes **5a** and **5b** were obtained in good yields (69 and 78% respectively) without particular difficulties. Their complete and straightforward syntheses are illustrated on the scheme 1.

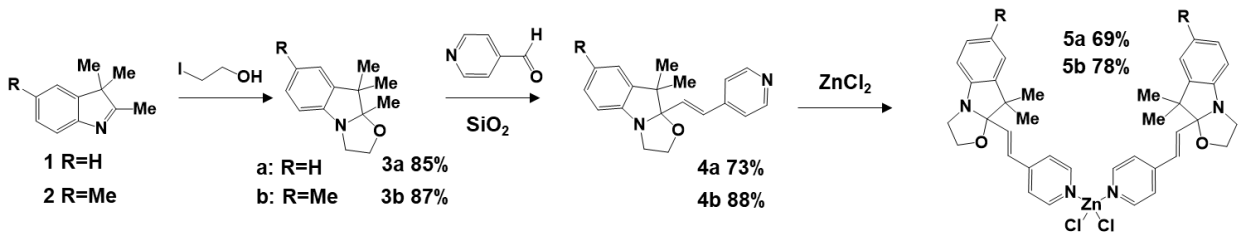

Scheme 1. Representation of the synthetic pathways to obtain the different Zn(II) metal complexes

3.2. Switching properties of free ligands

Before investigating properties of transition metal complexes, the multimodal commutabilities of the free ligands have been characterized. Indeed, due to the presence of a pyridine moiety acting as a weak base (pKa~ 5,23), their properties, especially their acidochromic properties could strongly be affected. Thus, depending on the open/closed status of the BOX and on the pyridine protonation (scheme 2), 4 different states should be envisioned for each ligand.

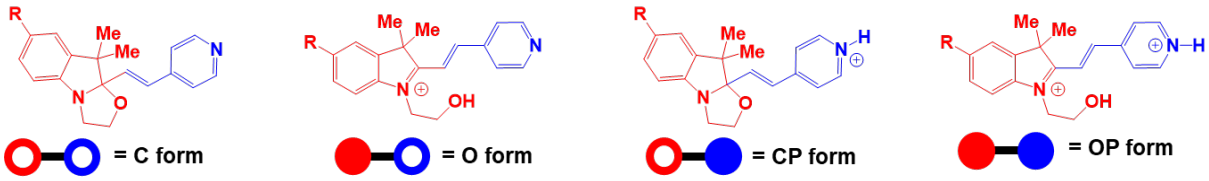

Scheme 2. Representation of the 4 different states of the dyad BOX-Pyridine depending on the open (O) or closed (C) status of the BOX unit and the protonation (P) of the pyridine moiety

Acidochromic properties. To monitor the switching properties of such system, UV-Visible spectroscopy represents certainly the most convenient technique as the opening of the oxazolidine ring comes with an enhancement of the conjugation as the hybridation of the carbon in position 2 changes from sp^3 to sp^2.[25] Under their closed form (C), compounds **4a** and **4b** are characterized by an absorption band centered at 243 and 245 nm respectively highlighting the poor influence of the indoline substituent in position 5 in agreement with previous studies on BOX derivatives.[35] As expected, a strong modification of the UV-Visible absorption spectra is observed in both cases as soon as the stimulation of the system starts by addition of increasing hydrochloric acid aliquots (figure 1).

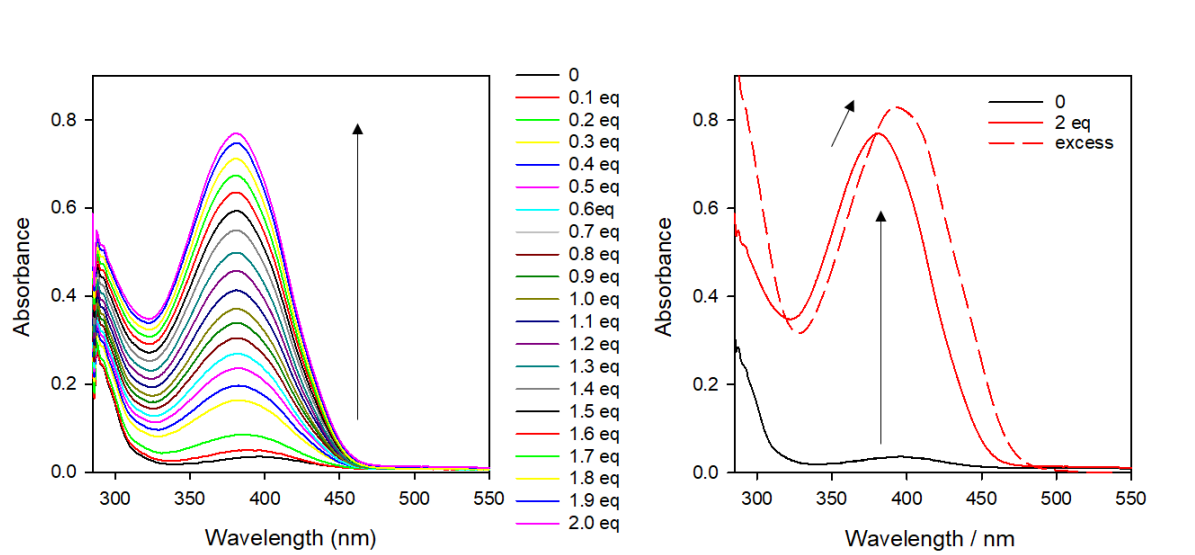

Figure 1. Evolution of the UV−visible absorption spectrum of **4b** in acetonitrile (0.05 mM) upon addition of HCl aliquots.

Indeed, one can observe that, due to the gradual increase of a unique intense band centered on 381nm (figure 1, left) upon the acidification with HCl, the **4b** solution turns deep yellow. As a continuous increase of the band at 381 nm up to 2 equivalents is observed, it is important to notice the absence of any isosbestic point. It can be then presumed that the stimulation of the system under its closed form is not selective and leads randomly to the BOX opening and pyridine protonation. As a consequence, this stimulation leads to a complex mixture of four different states of the compound (**C**, **CP**, **O** and **OP**). At the opposite, the small 14 nm bathochromic shift (λ_{max}=395 nm) observed upon addition of a large excess of acid (figure 1, right) could translate the full conversion of the molecular system to its **OP** form. This hypothesis is supported by theoretical study based on the density functional theory (DFT) and by its time dependent extension (TD-DFT) using B3LYP-6.311 G(d) as basis with IEFPCM solvation model. Figure 2 gathers the simulated spectra for all 4 different forms of ligand **4b**.

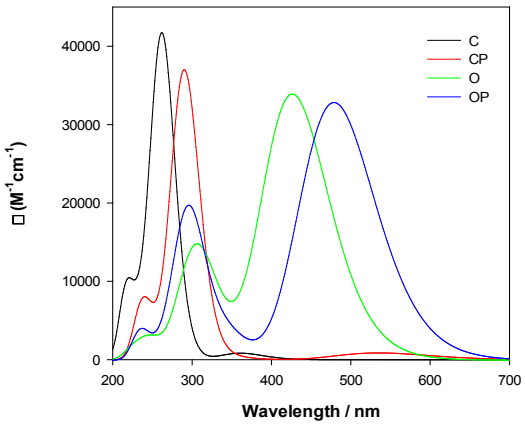

Compound 4b	*Wavelength (nm)*	*f*
C	*272* *261*	*0.195* *0.612*
CP	*291* *270*	*0.789* *0.039*
O	*427* *313* *292*	*0.833* *0.257* *0.145*
OP	*480* *301* *281*	*0.724* *0.310* *0.109*

Figure 2. Left: Simulated UV−visible absorption spectra. Right: most intense transitions (f >0.1) computed by B3LYP-6.311+G(d) methodology for free ligand **4b** under its **C**, **CP**, **O** and **OP** forms**.**

As expected, theoretical calculations indicate that only forms exhibiting an open BOX (**O** and **OP** forms) should exhibit an absorption band in the visible range. Indeed, the protonation of the pyridine moiety (CP form) should only undergo a slight bathochromic (30 nm) shift from the **C** form. Similar behavior seems occurring once the BOX is opened as a 60 nm bathochromic shift between **O** and **OP** forms is predicted. As a consequence, it can be assumed that the coloration changes of the solution upon the acidification result from the formation of both open forms (**O** and **OP**) which should be in equilibrium with the two closed forms (**C** and **CP)**.

Nevertheless, as the pyridine already presents a weak basicity, this later is known to decrease when substituted with an electron withdrawing group.[36] Thus, in these conditions, it is reasonable to assume that this weakness may justify the large excess of acid necessary to displace the equilibrium toward the full conversion of **C** to **OP** form translated on the UV-Visible spectra by a bathochromic shift. To summarize, we can presume that the addition of HCl to a solution of ligands under their closed form leads in a first place to a mixture of **C**, **CP** and **O** forms in

equilibrium, which is displaced to **OP** formation when the addition is pushed further as shown on scheme 3.

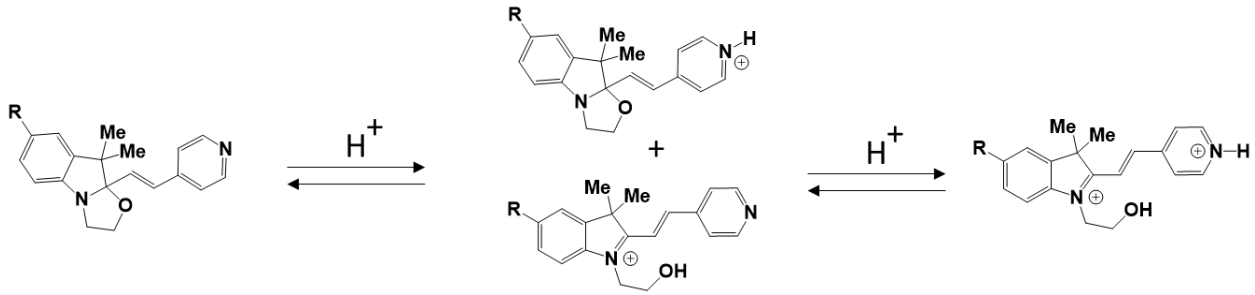

Scheme 3. Representation of the responsiveness of the ligand under stimulation by acid

In this context, the NMR spectroscopy has been used to unambiguously confirm the unselective competition between pyridine protonation and BOX opening under pH changes. Requiring higher concentration and not limited by solvent wavelength cut-off value, acetonitrile was advantageously replaced by DMSO to carry this study due to some solubility issues. As exemplified for compound **4b** on figure 3, the ^{1}H NMR spectra of both free ligands present typical signature of BOX derivatives under their closed forms such as: (*i*) two doublets (6.66 and 6.79 ppm) with a 16 Hz vicinal constant coupling confirming the trans isomery of the compounds; (*ii*) three singlets (1.05, 1.36 and 2.23 ppm) assigned to each methyl group and (*iii*) some multiplets between 3.2 and 3.8 ppm arising from the methylenic protons of the constrained oxazolidine cycle. These last are completed by two doublets (7.53 and 8.52 ppm for compound **4b**, figure 3) assigned to the pyridine unit.

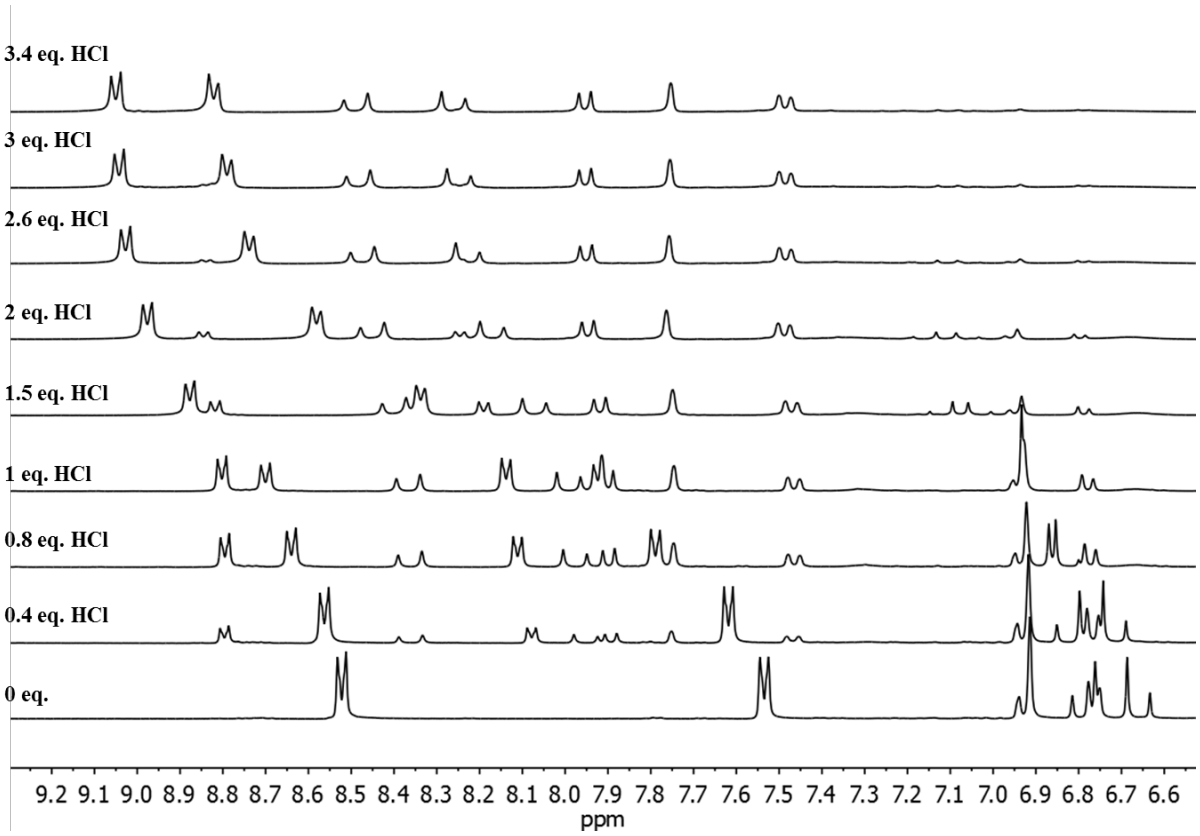

Figure 3. ^{1}H NMR spectra upon titration of **4b** (14 mM) by HCl in DMSO-d^{6} at 20°C up to 3.4 equivalents

As expected, the appearance of a new set of signals as soon as the addition of acid aliquots starts (figure 3) demonstrates the opening of the BOX unit and the formation of **O** form. This latter is clearly identified by the large downfield shift of the two doublets assigned to the ethylenic bridge from 6.66 and 6.79 ppm to 7.97 and 8.35 ppm. Concurrently, the characteristic peak-intensities of **C** form signals decrease and a gradual displacement of the corresponding aromatic signals to higher chemical shifts is noticed. As example, both doublets assigned to pyridine protons initially at 8.52 and 7.53 ppm are low field shifted to 8.70 and 7.92 ppm, respectively, after addition of one equivalent of HCl. As already observed for other pyridine derivatives,[37] such behavior translates a fast equilibrium at the NMR time scale between the closed (**C**) and the protonated closed (**CP**) forms. Up to one equivalent, the signals position assigned to the **O** form are not affected by the addition of acid. It is necessary to push further the addition of acid to observe

their shift to lower field. As a consequence, it can be concluded that the pyridine/pyridinium equilibrium is still effective once the oxazolidine ring is opened but exhibits a lower pKa value due to the generation of an indoleninium acting as a strong withdrawing group. As we can see on figure 3, 3.4 equivalents of acid are required to reach a stationary point corresponding to the full conversion of the compound to its protonated open form (**OP**). As suggested by UV-Visible spectroscopy, we can then confirm that the stimulation of the free ligands under their closed form by pH changes leads primarily to a mixture **CP** and **O** forms in equilibrium which is displaced by further stimulation to **OP** formation (scheme 3).

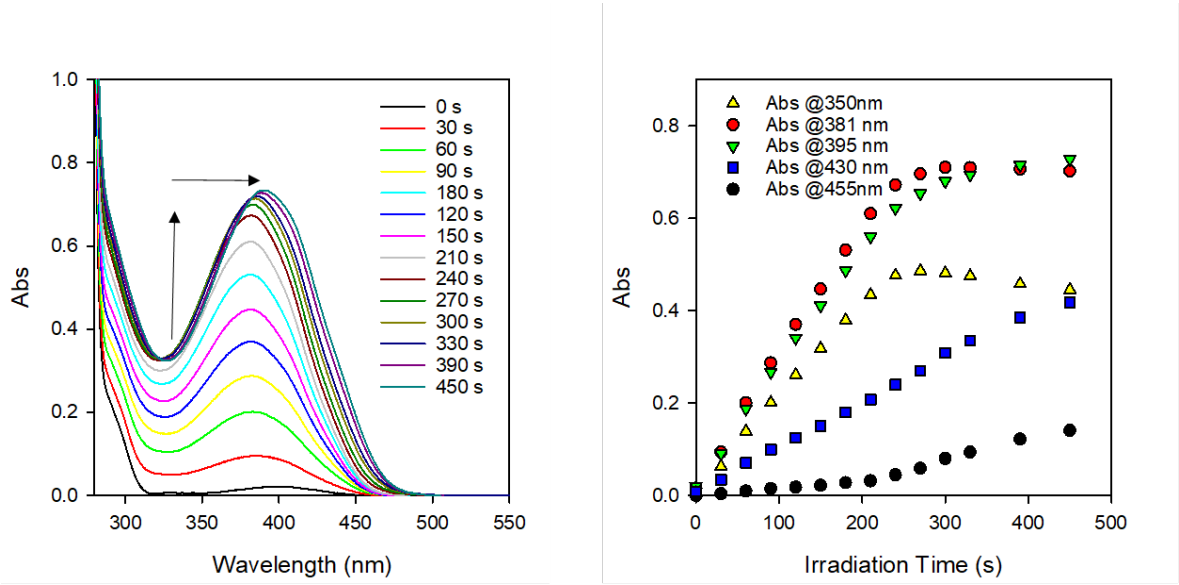

Figure 4. Left: UV-Visible spectrum changes of a solution of **4b** (0.05mM) under its closed form in a mixture ACN/PhCl (90/10) upon irradiation at 254 nm. Right: Corresponding evolution of the absorbance at different wavelengths.

Photochemical properties. On the basis of our previous works on BOX derivatives,[35] solution of free ligands in acetonitrile have been irradiated with 254 nm light in the presence of chlorobenzene (PhCl, 10%). As expected, the UV irradiation leads to the strong coloration of the solution reaching a photostationary state after few minutes. As example, the UV-Visible spectrum changes of a **4b** solution under UV irradiation is presented on figure 4. The strong similarity of the UV-visible spectra obtained by either irradiation or acidic titration allow us to

conclude that both stimulations trend at the end to the same state (**OP** form) and then, confirms the multi-modal switching abilities for this kind of ligands.

Importantly, one can observe on figure 4 (right) two stages in the evolution of the UV-Visible spectrum changes under UV irradiation. For short irradiation time (t< 270s), the appearance of a new broad absorption band centered at 381nm is observed which was assigned to the generation of the open form (**O**). Under prolonged irradiation time, additional hyper- and bathochromic shifts of the visible absorption band (395 nm) are observed and, as under acid stimulation, can be assigned to the generation of the **OP** state.

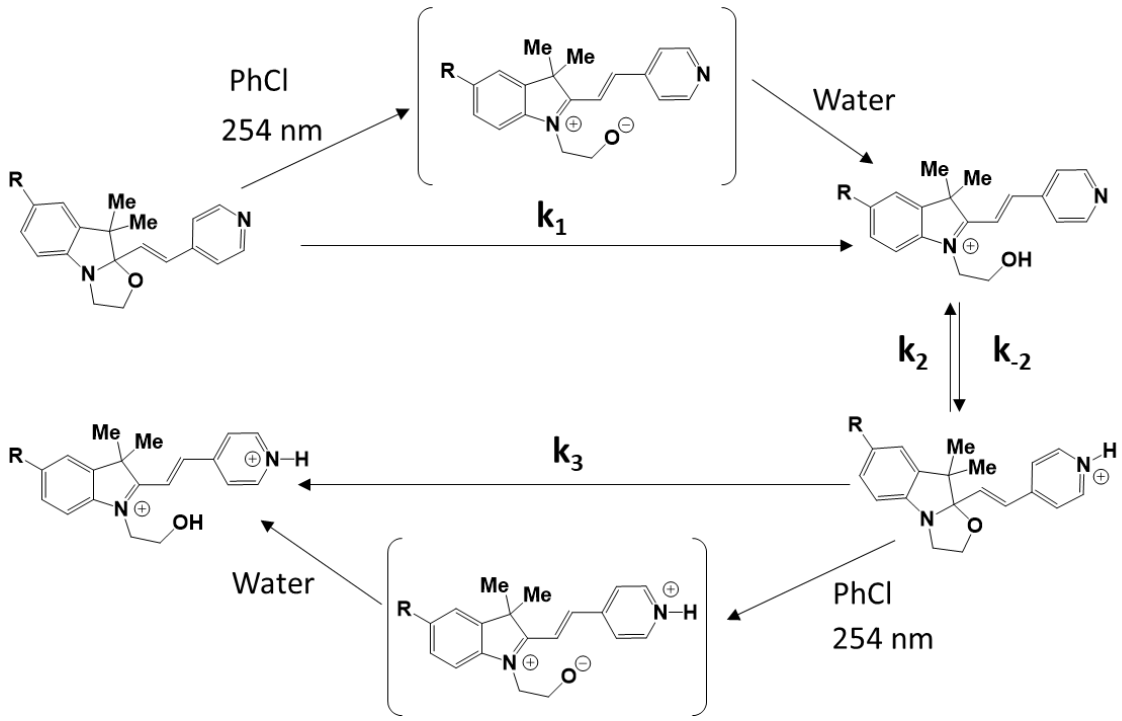

Scheme 4. Representation of the responsiveness of the ligand under stimulation by UV light including two irreversible photochemical processes and one equilibrium

To explain the generation of **OP** form under UV irradiation, one may first consider that the action of chlorobenzene as photosensitizer for BOX opening is known since the first report of their photochemical properties.[38, 39] If the photochemical process is still not fully elucidated, it is admitted that a photo-induced electron transfer between compounds results in the opening of the

oxazolidine ring and the generation of the corresponding zwitterionic form which is instantaneously converted in **O** form by trapping a proton from surrounding media (especially water traces). Photochemically inactive, this species seems involved in a tautomeric equilibrium with the **CP** form which can again undergo a similar photochemical process with photo-excited chlorobenzene. The proposed route leading to the conversion of **C** to **OP** form under UV irradiation is illustrated in the scheme 4.

Based on this hypothesis in which each individual step acts as a pseudo first order reaction, it is possible to describe the variation of each species as function of 4 kinetic constants.

$$\frac{d[C]}{dt} = -k_1[C] \quad (1)$$

$$\frac{d[O]}{dt} = k_1[C] + k_{-2}[CP] - k_2[O] \quad (2)$$

$$\frac{d[CP]}{dt} = k_2[O] - (k_3 + k_{-2})[CP] \quad (3)$$

$$\frac{d[OP]}{dt} = k_3[CP] \quad (4)$$

Equation (1) is easily solved by well-known first order integrated rate law: $[C] = [C]_0 e^{-k_1 t}$. Moreover, if one considers **CP** as an intermediate, it is possible to apply quasi-stationary state approximation. As a consequence, the equation (3) and (4) become

$$\frac{d[O]}{dt} = k_1[C]_0 e^{-k_1 t} + k_2[O]\left(\frac{k_{-2}}{(k_3+k_{-2})} - 1\right) \quad (5)$$

$$\frac{d[OP]}{dt} = \frac{k_2 k_3}{(k_3+k_{-2})}[O] \quad (6)$$

After resolution of both differential equations, the concentration of O and OP can be expressed as function of time and the different kinetic as following:

$$[O] = \frac{k_1(k_{-2}+k_3)[C]_0 e^{-k_1 t}}{k_1(k_{-2}+k_3)-k_2 k_3}\left(e^{\frac{(k_1(k_{-2}+k_3)-k_2 k_3)}{k_{-2}+k_3}t} - 1\right) \quad (7)$$

$$[OP] = \frac{k_1[C]_0 e^{-k_1 t}}{k_1(k_{-2}+k_3)-k_2 k_3}\left(-k_1(k_{-2}+k_3)e^{\frac{(k_1(k_{-2}+k_3)-k_2 k_3)}{k_{-2}+k_3}t} + e^{k_1 t}(k_1(k_{-2}+k_3)-k_2 k_3) - k_2 k_3\right) \quad (8)$$

As only O and OP forms should absorb in near-visible and visible spectral range (*vide infra*), the evolution of the spectrum under UV irradiation was fitted in this region by expression (9) in order to support our hypothesis and estimate the different kinetic constants.

$$Abs(\lambda) = \varepsilon_O^{\lambda}\,[O] + \varepsilon_{OP}^{\lambda}[OP] \qquad (9)$$

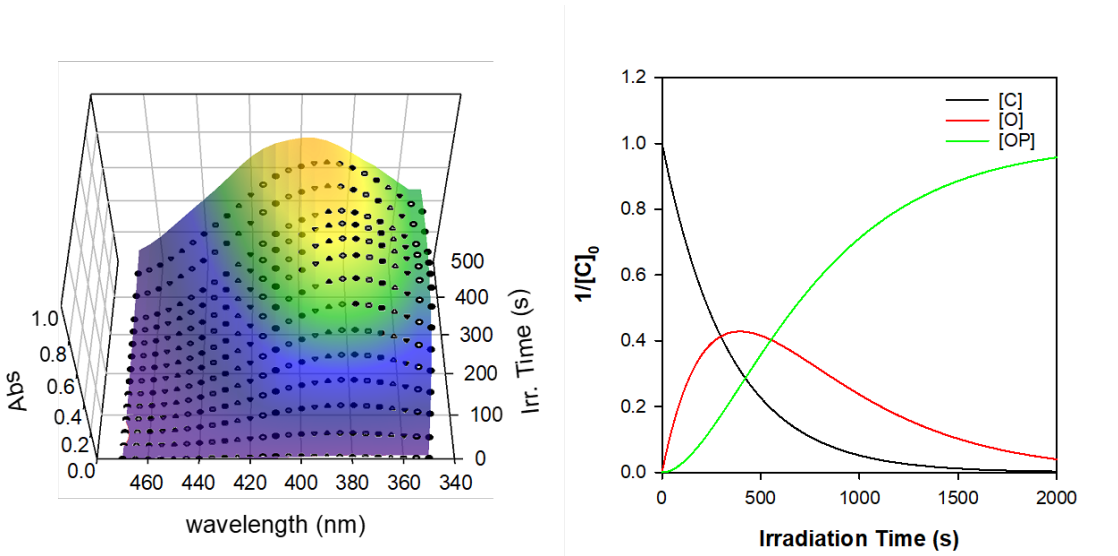

Figure 5. Left: Fitting of the evolution the absorption spectra (350-470 nm) by equation (9). Right: Resulting simulation of the evolution of [C]; [O] and [OP] as function of the irradiation time.

As one can notice (Figure 5), the experimental evolution of the absorption spectrum is nicely reproduced allowing to estimate the two kinetic constants of photoinduced ring opening processes to 3.10^{-3} and 7.10^{-6} s^{-1} for k_1 and k_3 respectively. The drastic decrease of photoreactivity between **C** and **CP** can be explained by the reinforcement of the electron withdrawing ability of the pyridine by its protonation which reduces the stability of the corresponding open form. The equilibrium constant between **O** and **CP** forms, k_2/k_{-2}, is estimated around ~ 250. It suggests then the quick and efficient transformation of the photogenerated specie **O** issued from the first opening to **CP** form which is available to undergo a second photochemical process leading to final **OP** form. In this context, despite a difference by almost 3 order of magnitude between both

kinetic constants, the switching of free ligand under light stimulation occurs in a stepwise manner but unfortunately with an insufficient selectivity as illustrated by the simulated evolution of **C**, **O** and **OP** forms as function of irradiation time (figure 5).

Electrochromic properties. As mentioned earlier, the opening of the oxazolidine ring can be also induced by an electrochemical process. Noteworthy, this later requires the presence of a substituent in position 5 of the BOX to avoid undesirable C-C oxidative coupling.[40] In this context, the electrochemical behavior of ligands **4b** and **5b** has been investigated by cyclic voltammetry (CV) and their voltammograms are presented in figure 6.

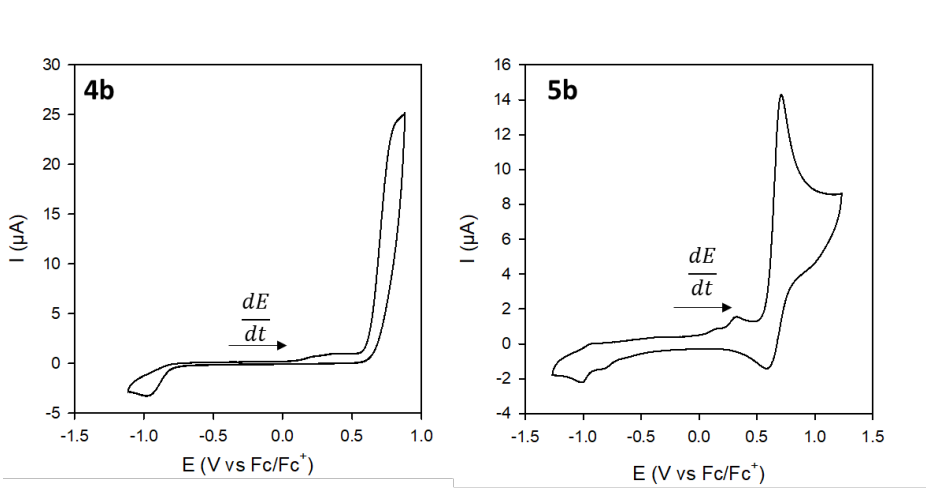

Figure 6. Cyclic voltammograms of derivatives **4b** (0.62 mM) and **5b** (0.57 mM) in 0.1 M $TBAPF_6/CH_3CN$ solution at 100 $mV.s^{-1}$.

As expected, compound **4b** exhibits a non-reversible oxidation process at 0.74 V *vs* Fc/Fc^+ which generates a new system as translated by the appearance of a non-reversible reduction process (-0.88 V) on the scan back. In agreement with our previous studies,[35, 40] this typical electrochemical behavior indicates that the oxidation of the **C** form is mainly localized on the indoline unit leading to corresponding radical cation which undergoes a chemical process leading to the opening of the oxazolidine ring. In similar way, the reduction process seems assigned to the electrochemical closing from **O** to **C** form. Interestingly, in the present case, an important difference of charge exchanged between oxidation (**C** to **O**) and reduction (**O** to **C**) processes is observed. Once again, the tautomeric equilibrium between **O** and **CP** forms can explain this

behavior. Indeed, it can be suggested that the oxidation of the **C** form leads to the generation of the **O** form which is partially converted to **CP** form due to the tautomeric equilibrium (*vide supra)*. Acting independently from the pyridinium unit when the oxazolidine ring is closed, the BOX moieties should be also able to undergo an oxidation process at a close oxidation potential, leading the corresponding radical cation and, at the end, to the **OP** formation. In fact, this hypothesis is supported by theoretical calculations.

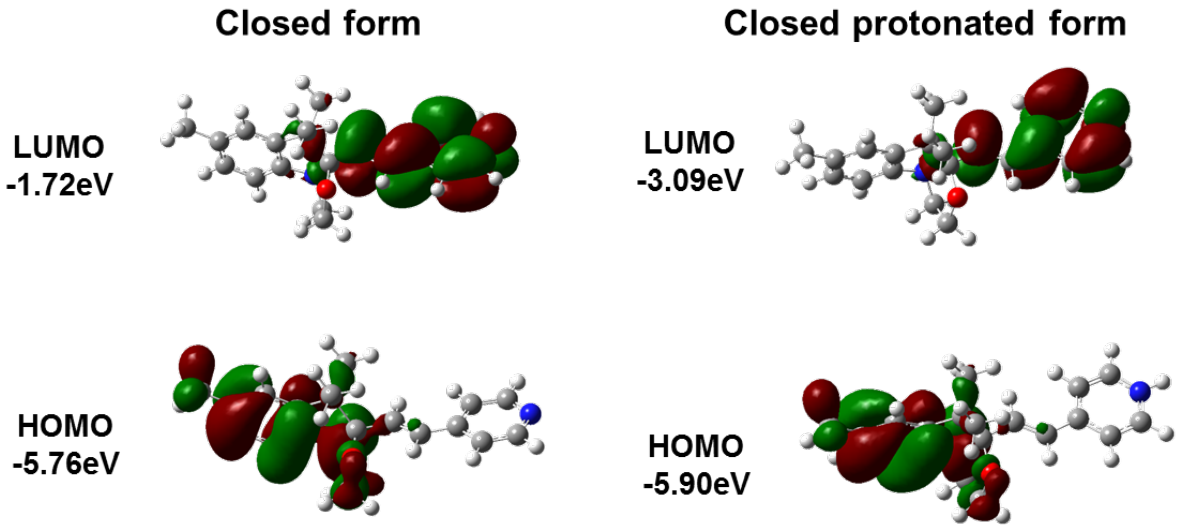

Figure 7. Molecular orbitals and energies of compound **4b** under its **C** (left) and **CP** (right) forms calculated at the B3LYP/6-311G(d) level with IEFPCM (ACN) solvation model

As represented on figure 7, the HOMO of compound **4b** is mainly localized on the BOX unit for both **C** and **CP** forms. In addition, the variation of HOMO energy level due to the pyridine protonation appears quite limited (0.14eV) and not sufficient to induce an important variation of oxidation potential. As a consequence, the electro-switching of system occurs in two simultaneous steps: the **C** to **O** transformation and the conversion from **CP** to **OP** happen then at close potentials. Thus, contrary to other molecular systems including several BOX units[41] which allow observation of two well resolved oxidation processes, this poor difference leads to

an unselective wide oxidation wave including both processes. This assumption is confirmed by the titration of compound **4b** using $NOSbF_6$ as an oxidizing reagent.

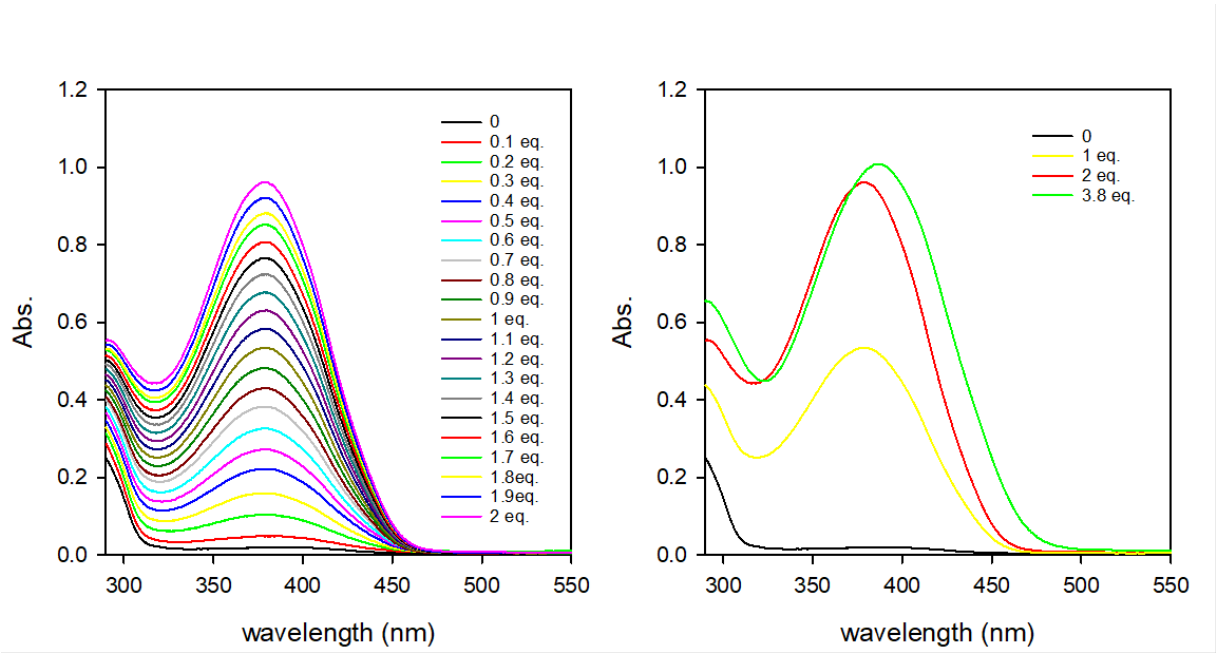

Figure 8. UV-Visible spectrum changes of a solution of **4b** in ACN (0.05mM) upon addition of $NOSbF_6$.

As one can observe on figure 8, the UV-visible spectra obtained by $NOSbF_6$ or acidic titration appear very similar, then translating that both stimulation leads to the same transformation, and then, confirming the multi-modal switching abilities of these molecular systems. More important, a bathochromic shift of the maximum absorption wavelength from 381 to 395 nm is noticed when a slight excess of oxidant is added. Assigned to the full conversion from **C** to **OP** form, it translates that, as under acidic conditions, an overstimulation is requisite to counteract the tautomerism between **O** and **CP**.

3.3. Switching properties of corresponding zinc complexes.

Structure of the zinc complexes. If the introduction of a transition metal ion in the close vicinity of a multimodal switchable unit such as BOX could open new prospects, the elaboration of such

complexes stays, to the best of our knowledge, unreported. Since the coordination unit used here is a monodentate ligand (pyridine), the use of Zn(II) metal cation shouldn't affect the molecular structure of the BOX based ligand.

In order to support this hypothesis, comparative X-ray diffraction studies between free ligand **4b** and corresponding zinc(II) complex **5b** were carried out. For both, selected parameters of the X-ray diffraction data collection and refinement are provided in SI, as well as selected bond lengths and angles.

As expected, the coordination of the ligand by the zinc(II) induces only slight modifications of its structure. Except different space group ($P2_1\ 2_1\ 2_1$ and *C 2/c* for **4b** and **5b** respectively), free ligand and complex exhibit one independent molecule in the unit cell. With a stoichiometry of 2:1, the zinc ion is tetracoordinated presenting a distorted tetrahedral coordination sphere formed by two pyridine nitrogen atoms and two chlorine atoms.

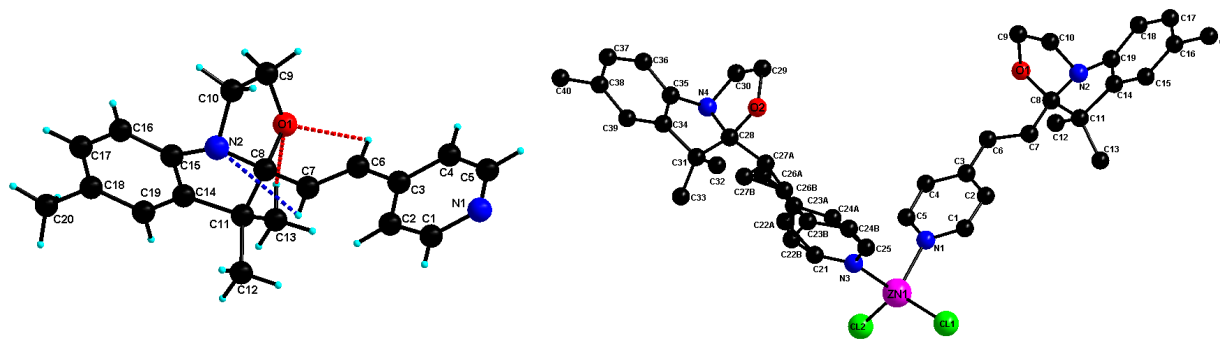

Figure 9. Crystal structure and atom numbering of free ligand **4b** (left) and its corresponding zinc(II) complex **5b** (right)

As suggested by theoretical calculations, the ligand is not planar. Changing from 86.67 (2)° in free ligand to 74.77 (2)° and 69.41 (2)° in complex, metal binding has only a moderate effect on the dihedral angle between the phenyl and pyridine planes. In similar way, bond lengths within the pyridine and phenyl units do not differ substantially from one species to the other. However, a disorder of carbon atoms can be highlighted in the complex as seen in figure 9. To explain this difference, it can be suggested that the molecular conformation of free ligand is stabilized by

strong intramolecular C–H···O and C–H···N, (C6–H6···O1 2.415 (0) Å and C13–H13A···O1 2.379, C7–H7···N2 2.717) hydrogen bonds (figure 9). Furthermore, each molecule interacts with adjacent molecules by one non-conventional hydrogen bonds C–H···N, (C2–H2···N1, 2.544(0) Å), and two hydrogen bonds C–H···π from phenyl ring and from pyridine fragment respectively (C4–H4···π (2.712 (0) Å, C13–H13B···π (2.853(0) Å), as illustrated in Figure 10. These interactions lead to the formation of 3D supramolecular layers parallel with the *bc* crystallographic plane (figure 3).

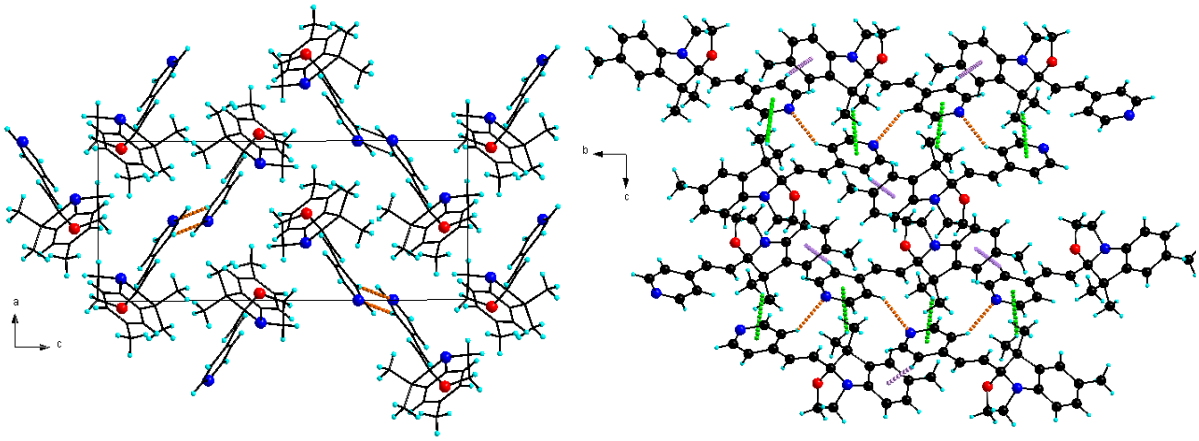

Figure 10. Perspective view of **4a** ligand in the *ac* (left) and *bc* (right) planes showing the two types of interactions C–H···N hydrogen bonds (orange dashed lines), C–H···π interactions, from phenyl ring (purple dashed lines) and from pyridine fragment (green dashed lines)

Concerning corresponding zinc(II) complex **5b,** RX diffraction of does not reveal any intra- or inter-molecular hydrogen bond involving the pyridine moiety. In place, C–H···*π* intermolecular interactions (H40···centroid 2.819 (2) Å and H20B···centroid 2.640 (2) Å) along the *a* axes and short intermolecular C–H···Cl contacts (C10–H10···Cl1= 2.691(2) Å) are evidenced, resulting in a supramolecular chain parallel to the crystallographic *c* axis (figure 11).

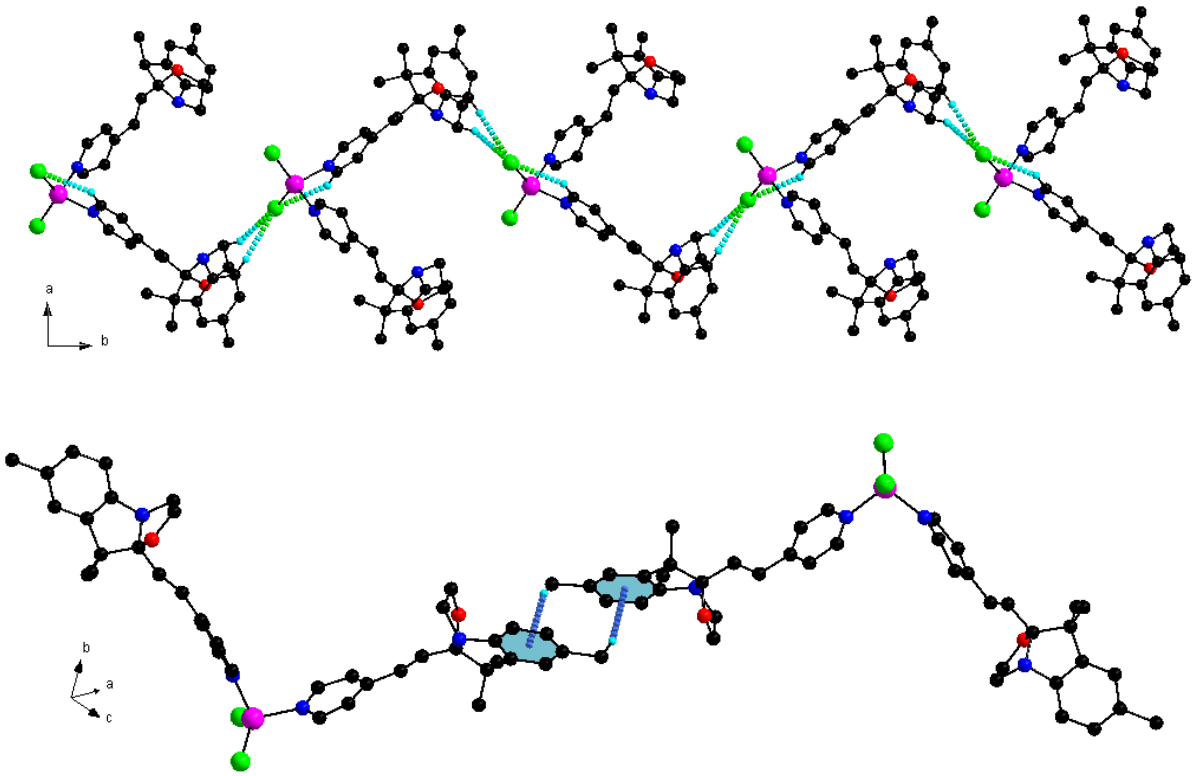

Figure 11. Perspective of the supramolecular chain generated by hydrogen bonding C–H···Cl (green-cyan dashed lines) in complex **5b** in the ab plane (top), and those reinforced by C–H···π interactions (blue dashed line, bottom)

More important, X-Ray studies confirm that BOX units are not involved inside the coordination sphere of the metallic ion and that their own structure are not affected by the metal binding. On this basis, it can be then presumed that the switching abilities of the ligand will be preserved once the complex formed. This assumption is perfectly supported by *ab initio* quantum calculations (B3LYP/6.311G(d)). As example, complex **5b** exhibits quasi-degenerated HOMO and LUMO orbitals, similar in energy and localization to that observed for free ligand **4b** (see SI).

In this context, it is not surprising to observe only a slight variation of the optical properties between the free ligand and corresponding complexes. As shown on figure 12 for **4b** and **5b**, the zinc complexation doesn't induce any strong variation of the absorption maximum wavelength (245nm) but logically leads to twice the extinction coefficient (28.7 10^3 and 56.3 10^3 $L.mol^{-1}.cm^{-}$

[1] for compound **4b** and **5b** respectively). Noteworthy, an hyperchromic effect was observed in the 260-290 nm range with the complexation. By following the absorption at 280 nm of a solution of 4b upon the addition of $ZnCl_2$ aliquots, it is possible to confirm the 2:1 stoichiometry of the complex and its stability in diluted conditions.

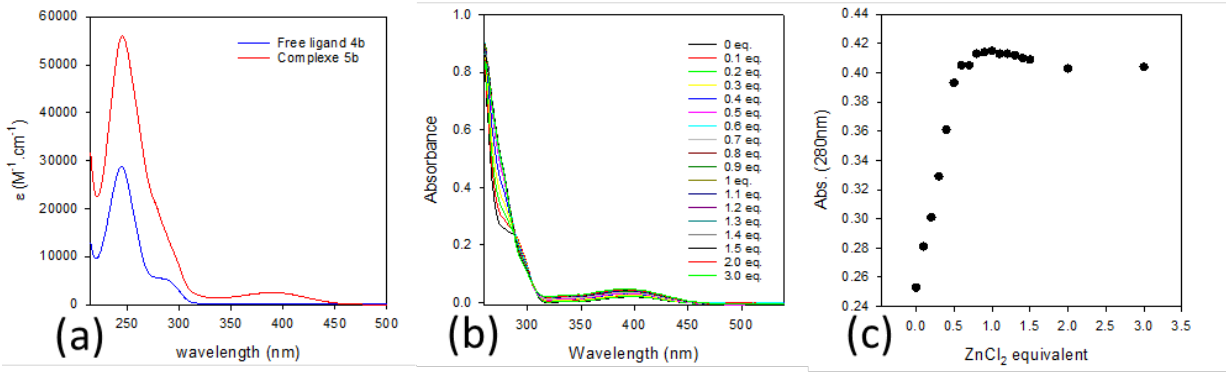

Figure 12. (a) UV visible spectra of free ligand **4b** and corresponding zinc complex **5b** in the ACN. (b) Variation of UV-Visible spectrum of **4b** (0.03mM) in ACN upon the addition of $ZnCl_2$ aliquots. (c) Evolution of the absorbance at 280 nm upon addition of $ZnCl_2$.

As performed with free ligands, the switching abilities of corresponding zinc(II) complexes were investigated by monitoring the evolution of the system by UV-Visible spectroscopy when stimulated by acid, light and oxidant.

Acidochromic properties. As observed with free ligand, a strong modification of the UV-Visible absorption spectra is observed as soon some acid aliquots are added. As presented for compound **5b** in figure 13, acidification of the solution leads to formation of an intense broad band centered at 381 nm. Based on previous study on free ligand, this coloration is assigned to the BOX opening (*vide infra*). Analogously to **4b**, starting from corresponding zinc complex, adding 4 eq. of acid is necessary to attain stabilized spectroscopic properties. Here also, this excess of acid induces a slight hyperchromic and bathochromic shift of the absorption maximum wavelength.

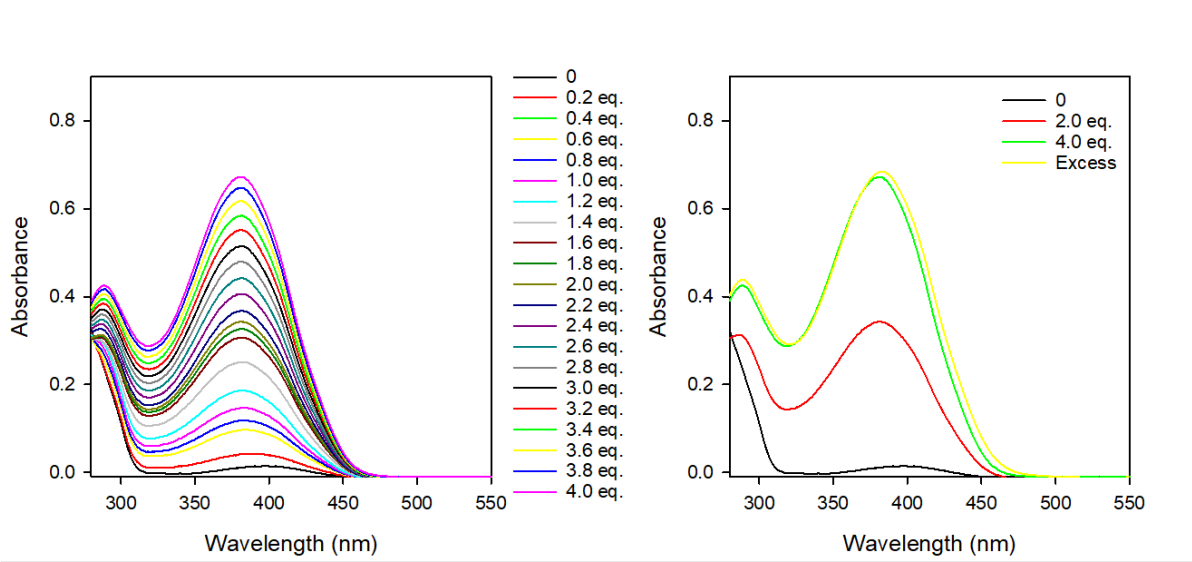

Figure 13 : Evolution of the UV−visible absorption spectrum of **5b** in acetonitrile (0.02 mM) upon addition of HCl aliquots.

As, no isosbestic point is observed during this addition, these similarities let presume (*i*) a complete independence of both BOX units grafted on the metal center, and (*ii*) the presence in solution of more than two species in equilibrium. It could suggest that, again, a tautomeric equilibrium between an opened and a protonated closed form occurs. Thus, it is worth to suppose that, whatever the external stimulation, the opening of the BOX is accompanied by the pyridine protonation and, then, by the complex dissociation and zinc cation release.

To clarify this point, ^{1}H NMR titrations were performed in d^{3} ACN. The gradual addition of acid leads to observe *i*) the decrease of initial closed form signals and concomitant appearance of new resonances assigned to the open form of the complex and *ii*) the formation of a precipitate suggesting the formation of CP and, as consequence, the complex dissociation. To support this hypothesis, it is important to note that the partial acidic stimulation of the free ligand **4b** also leads to observe similar precipitate formation in ACN. Furthermore, when an excess $ZnCl_2$ is added to a mixture of **O** and **CP** forms of **4b** in equilibrium, the precipitate disappears and ^{1}H NMR spectroscopy confirms the formation of corresponding zinc(II) complex under its **O** form

(see S.I.) Finally, the addition of an excess of acid induces the complete dissociation of **5b** leading to the exclusive formation of free **4b** under its **OP** form (as shown below).

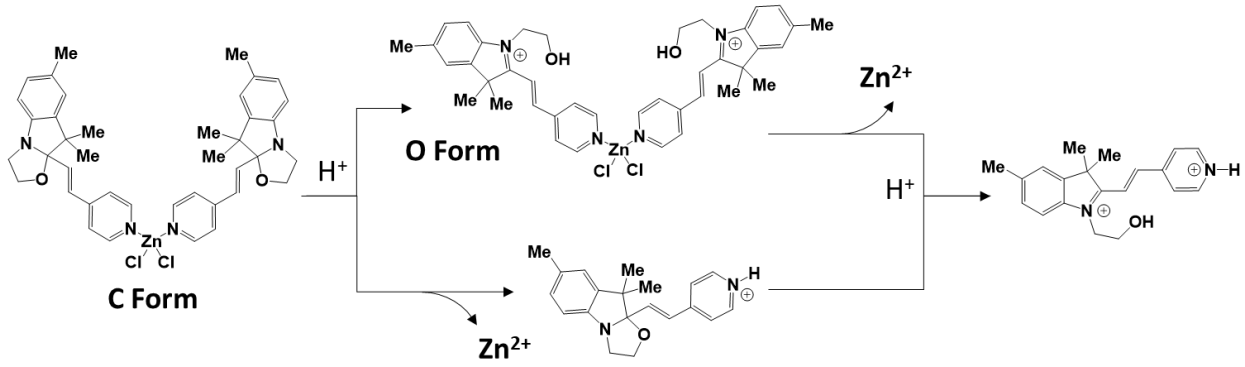

Scheme 5. Proposed route leading to the zinc ion release from BOX based complexes under an acidic stimulation

To conclude, the metal binding did not affect strongly the acidochromic properties of the ligand. As a consequence, the tautomeric equilibrium between **O** and **CP** forms is still present and leads to observe the Zn release as soon as the complex is under acidic stimulation.

Release of Zinc ion under photo- or electro-stimulation. The multimode switchable ability of the BOX suggests the possibility to release zinc ion under milder stimulation than addition of acid. In order to verify this assumption, the light (254nm) and electrochemical ($NOSbF_6$) stimulations of zinc complexes were carried out and monitored by UV-Visible spectroscopy.

As represented on figure 14 for compound **5b**, both stimulation leads to strong yellow coloration of the solution and to the appearance of a unique band centered at 381 nm. In addition, a typical slight hyper and bathochromic shift is noticed for longer irradiation time or more than 2 eq. of chemical oxidant is added. As expected, a perfect overlap of UV-Visible spectra is observed whatever the nature of the stimulation. It can be then concluded that this molecular system reaches an identical final state in all cases. Assigned to the formation of **OP** form, it implies the zinc ion release under acido-, photo- and electro-stimulation.

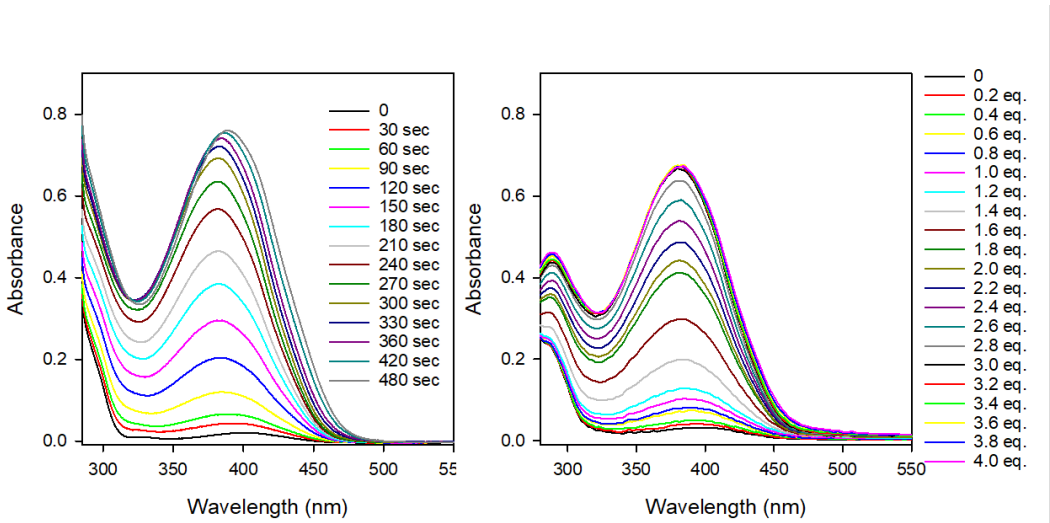

Figure 14. UV-Visible spectrum changes of a solution of complex **5b** in ACN (0.02mM) upon irradiation at 254 nm in presence of PhCl 10% (left) and $NOSbF_6$ (right)

Concerning the electro-stimulation, the presence of two redox active ligands in close vicinity raises the question of their possible selective addressability and the possibility to form mixed valences species. For this reason, the complex **5b** was studied by CV. According to figure 6, the cyclic voltammogram of **5b** exhibits one pseudo non-reversible oxidation wave at 0,72V very close to the free ligand oxidation process at 0.74V what underlines an equivalent environment. More important, it was not possible to observe any splitting of the oxidation peaks, which translates the perfect electronic equivalence of both BOX units and then their independent opening.

In comparison to the free ligand, the observation of a full non-reversible oxidation process requires to decrease the scan rate. Based on these results, we can assume that the kinetic rate leading to the opening of the BOX was decreased with the complexation of the Zn which probably also slows down the tautomeric equilibrium leading to the **CP** form.

4. Conclusion

In summary, we have demonstrated that the successful combination of a BOX unit with a *nitrogen*-containing heteroarene, as simple as a pyridine, leads to a new class of multi-addressable ligands exhibiting multimodal switching abilities. Based on this, a first set of BOX based coordination complexes **5a-b** have been synthesized and characterized allowing to

demonstrate that the acido-; electro- and photoswitching properties of the BOX moiety are perfectly maintained after metal-binding. Nevertheless, the moderate basicity of pyridine moiety conducts to observe a subtle and interesting tautomeric equilibrium between the open O form and the closed pyridinium protonated form CP of the system whatever the nature of the stimulation. More important, both of them lead to the same opened protonated OP form when stronger stimulation is applied. Due to some lability, this tautomeric equilibrium is not suppressed by metal binding. Therefore, upon all types of stimulation (photon, proton or electron), the BOX of complex **5** are opened and the pyridine motifs protonated leading to the obtainment of the OP form accompanied by the destruction of the complex and therefore release of zinc ion. At the opposite, a simple basic treatment of the mixture allows to restore the initial state what leads to the regeneration of the zinc complex. This possibility to catch and release the metal on demand by using two external and orthogonal stimulations represents a promising approach especially for studying the numerous biological processes involving zinc ions and, as consequence, requires further investigations.

Acknowledgments.

All authors thank the MATRIX SFR of the University of Angers for its help in the characterization of the different derivatives, especially Dr. Ingrid Freuze for mass spectrometry measurements, B. Siegler for NMR spectroscopy experiments. Dr. Awatef Ayadi is acknowledged for her help with X-Ray diffraction analysis. Finally, Dr. Y. Aidibi is very grateful to the Université d'Angers for its PhD granting.

References:

[1] Jiang G, Song Y, Guo X, Zhang D, Zhu D. Organic Functional Molecules towards Information Processing and High-Density Information Storage. Adv Mater. 2008;20(15):2888-2898.

[2] Sauer M. Reversible molecular photoswitches: A key technology for nanoscience and fluorescence imaging. P Natl Acad Sci USA. 2005;102(27):9433-9434.

[3] Sato O. Switchable molecular magnets. Proc Jpn Acad Ser B Phys Biol Sci. 2012;88(6):213-225.

[4] Nakatani K, Piard J, Yu P, Métivier R. Introduction: Organic Photochromic Molecules. Photochromic Materials : Preparation, Properties and Applications. 2016. p. 1-45.

[5] Irie M. Photochromism of diarylethene molecules and crystals. P JPN Acad B-Phys. 2010;86(5):472-483.

[6] Irie M, Fulcaminato T, Matsuda K, Kobatake S. Photochromism of Diarylethene Molecules and Crystals: Memories, Switches, and Actuators. Chem Rev. 2014;114(24):12174-12277.

[7] Rau H. Chapter 4 - Azo Compounds. In: Dürr H, Bouas-Laurent H, editors. Photochromism. Amsterdam: Elsevier Science; 2003. p. 165-192.

[8] Klajn R. Spiropyran-based dynamic materials. Chem Soc Rev. 2014;43(1):148-184.
[9] Kortekaas L, Browne WR. The evolution of spiropyran: fundamentals and progress of an extraordinarily versatile photochrome. Chem Soc Rev. 2019;48(12):3406-3424.
[10] Fihey A, Perrier A, Browne WR, Jacquemin D. Multiphotochromic molecular systems. Chem Soc Rev. 2015;44(11):3719-3759.
[11] Perrier A, Maurel F, Jacquemin D. Single Molecule Multiphotochromism with Diarylethenes. Acc Chem Res. 2012;45(8):1173-1182.
[12] Braslavsky SE. Glossary of terms used in photochemistry, 3rd edition (IUPAC Recommendations 2006). Pure Appl Chem. 2007;79(3):293.
[13] He X, Lagrost C, Norel L, Rigaut S. Ruthenium(II) σ-arylacetylide complexes as redox active units for (multi-)functional molecular devices. Polyhedron. 2018;140:169-180.
[14] Koike T, Akita M. Photochromic Organometallics: Redox-Active Iron and Ruthenium Complexes with Photochromic DTE Ligand. In: Irie M, Yokoyama Y, Seki T, editors. New Frontiers in Photochromism. Tokyo: Springer Japan; 2013. p. 205-224.
[15] Shen C, He X, Toupet L, Norel L, Rigaut S, Crassous J. Dual Redox and Optical Control of Chiroptical Activity in Photochromic Dithienylethenes Decorated with Hexahelicene and Bis-Ethynyl-Ruthenium Units. Organometallics. 2018;37(5):697-705.
[16] Guerchais V, Ordronneau L, Le Bozec H. Recent developments in the field of metal complexes containing photochromic ligands: Modulation of linear and nonlinear optical properties. Coord Chem Rev. 2010;254(21):2533-2545.
[17] Kume S, Nishihara H. Photochrome-coupled metal complexes: molecular processing of photon stimuli. Dalton T. 2008(25):3260-3271.
[18] Samanta S, Ghosh P, Goswami S. Recent advances on the chemistry of transition metal complexes of 2-(arylazo)pyridines and its arylamino derivatives. Dalton T. 2012;41(8):2213-2226.
[19] Hiroshi N. Multi-Mode Molecular Switching Properties and Functions of Azo-Conjugated Metal Complexes. B Chem Soc Jpn. 2004;77(3):407-428.
[20] Kurihara M, Nishihara H. Azo- and quinone-conjugated redox complexes—photo- and proton-coupled intramolecular reactions based on d–π interaction. Coord Chem Rev. 2002;226(1):125-135.
[21] Deo C, Bogliotti N, Métivier R, Retailleau P, Xie J. Photoswitchable Arene Ruthenium Complexes Containing o-Sulfonamide Azobenzene Ligands. Organometallics. 2015;34(24):5775-5784.
[22] Berben LA, de Bruin B, Heyduk AF. Non-innocent ligands. Chem Commun. 2015;51(9):1553-1554.
[23] Lorcy D, Bellec N, Fourmigué M, Avarvari N. Tetrathiafulvalene-based group XV ligands: Synthesis, coordination chemistry and radical cation salts. Coord Chem Rev. 2009;253(9):1398-1438.
[24] Riobé F, Avarvari N. Electroactive oxazoline ligands. Coord Chem Rev. 2010;254(13):1523-1533.
[25] Szalóki G, Sanguinet L. Properties and Applications of Indolinooxazolidines as Photo-, Electro-, and Acidochromic Units. In: Yokoyama Y, Nakatani K, editors. Photon-Working Switches. Tokyo: Springer Japan; 2017. p. 69-91.
[26] Gritzner G, Kuta J. Recommendations on reporting electrode potentials in nonaqueous solvents (Recommendations 1983). Pure Appl Chem. 1984;56(4):461-466.
[27] Sevez G, Gan J, Delbaere S, Vermeersch G, Sanguinet L, Levillain E, Pozzo JL. Photochromic performance of a dithienylethene-indolinooxazolidine hybrid. Photoch Photobio Sci. 2010;9(2):131-135.
[28] Tomasi J, Cammi R, Mennucci B. Medium effects on the properties of chemical systems: An overview of recent formulations in the polarizable continuum model (PCM). Int J Quantum Chem. 1999;75(4-5):783-803.
[29] Hayami M, Torikoshi S. Color-changing compounds. Matsushita Electric Industrial Co., Ltd., Japan . 1976. p. 46 pp.
[30] Szaloki G, Sanguinet L. Silica-Mediated Synthesis of Indolinooxazolidine-Based Molecular Switches. J Org Chem. 2015;80(8):3949-3956.
[31] Burgess J, Prince RH. Zinc: Inorganic & Coordination Chemistry In: King RB, Crabtree RH, Lukehart CM, Atwood DA, Scott RA, editors. Encyclopedia of Inorganic Chemistry. John Wiley & Sons, Ltd; 2006.

[32] Bang S, Lee Y-M, Hong S, Cho K-B, Nishida Y, Seo MS, Sarangi R, Fukuzumi S, Nam W. Redox-inactive metal ions modulate the reactivity and oxygen release of mononuclear non-haem iron(III)–peroxo complexes. Nat Chem. 2014;6(10):934-940.
[33] Tomasik P, Ratajewicz Z, Newkome GR, Strekowski L. σ-Pyridine Coordination Compounds with Transition Metals. Chem Heterocycl Compd. 1985.
[34] Guezguez I, Ayadi A, Ordon K, Iliopoulos K, Branzea DG, Migalska-Zalas A, Makowska-Janusik M, El-Ghayoury A, Sahraoui B. Zinc Induced a Dramatic Enhancement of the Nonlinear Optical Properties of an Azo-Based Iminopyridine Ligand. J Phys Chem C. 2014;118(14):7545-7553.
[35] Szaloki G, Aleveque O, Pozzo J-L, Hadji R, Levillain E, Sanguinet L. Indolinooxazolidine: a versatile switchable unit. J Phys Chem B. 2015;119(1):307-315.
[36] Hedidi M, Bentabed-Ababsa G, Derdour A, Halauko YS, Ivashkevich OA, Matulis VE, et al. Deprotometalation of substituted pyridines and regioselectivity-computed CH acidity relationships. Tetrahedron. 2016;72(17):2196-2205.
[37] Handloser CS, Chakrabarty MR, Mosher MW. Experimental determination of pKa values by use of NMR chemical shift. J Chem Edu. 1973;50(7):510-511.
[38] Petkov I, Charra F, Nunzi JM, Deligeorgiev T. Photochemistry of 2-[(1,3,3-trimethylindoline-2(1H)-ylidene)propen-1-yl]-3,3-dimethylindolino[1,2-b]-oxazolidine in solution. J; Photoch Photobio A. 1999;128(1-3):93-96.
[39] Petkov I, Charra F, Nunzi JM, Deligeorgiev T. Photo- and thermoinduced ring opening reaction of 2-[(1,3,3-trimethylindoline-2(1H)-yliden)propen-1-yl]-3,3-dimethylindolino[1,2-b]-oxazolidine in polymer films. Cent Eur J Chem. 2004;2(2):290-301.
[40] Hadji R, Szaloki G, Aleveque O, Levillain E, Sanguinet L. The stepwise oxidation of indolino[2,1-b]oxazolidine derivatives. J Electroanal Chem. 2015;749:1-9.
[41] Aidibi Y, Guerrin C, Alévêque O, Leriche P, Delbaere S, Sanguinet L. BT-2-BOX: An Assembly toward Multimodal and Multilevel Molecular System Simple as a Breeze. J Phys Chem C. 2019;123(18):11823-11832.

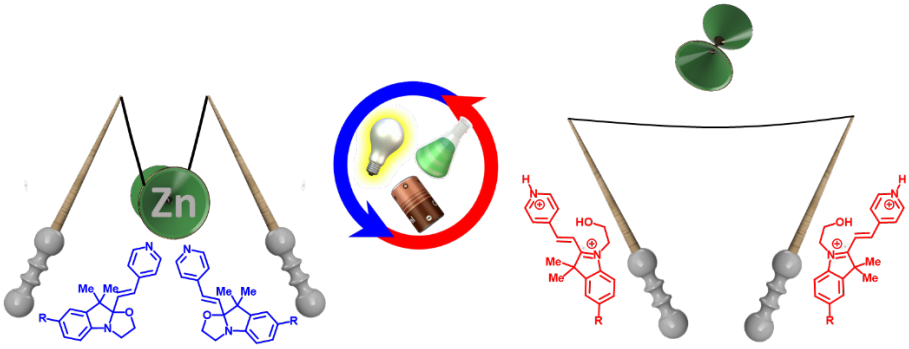
Zn
Me
Me
N
O
R
H
HO
OH